drones

MDPI

Article

Performance Analysis and Conceptual Design of Lightweight UAV for Urban Air Mobility

Francesco Mazzeo [1,†], Emanuele L. de Angelis [2,*,‡], Fabrizio Giulietti [2,‡], Alessandro Talamelli [2] and Francesco Leali [1]

[1] Department of Engineering "Enzo Ferrari", University of Modena and Reggio Emilia, 41121 Modena, Italy; francesco.mazzeo@unimore.it (F.M.); francesco.leali@unimore.it (F.L.)
[2] Department of Industrial Engineering, University of Bologna, 40126 Bologna, Italy; fabrizio.giulietti@unibo.it (F.G.); alessandro.talamelli@unibo.it (A.T.)
* Correspondence: emanuele.deangelis4@unibo.it
† Current address: Via P. Vivarelli, 10, 41125 Modena, Italy.
‡ These authors contributed equally to this work.

Abstract: In the present study, a performance analysis of three different VTOL configurations is presented within an urban air mobility context. A classical lightweight helicopter was employed as a reference configuration to design a dual-rotor side-by-side helicopter and a hexacopter drone layout. An analytical model based on general momentum and blade element theories was developed for single- and multiple-rotor configurations in horizontal and vertical flight conditions. Suitable battery pack and electric motor designs were produced to evaluate the endurance and range of the different configurations for a specific mission. This paper provides fundamental insights into the endurance and range capabilities of multiple-rotor unmanned aerial vehicles (UAVs) and a qualitative discussion on the safety and acceptability features of each configuration implemented in an advanced air mobility context. As a result, the side-by-side helicopter configuration was identified as the best solution to be introduced within urban environments, fulfilling all the performance and mission requirements.

Keywords: eVTOL; conceptual design; performance analysis; helicopter; UAV; side-by-side

Citation: Mazzeo, F.; de Angelis, E.L.; Giulietti, F.; Talamelli, A.; Leali, F. Performance Analysis and Conceptual Design of Lightweight UAV for Urban Air Mobility. *Drones* **2024**, *8*, 507. https://doi.org/10.3390/drones8090507

Academic Editor: Abdessattar Abdelkefi

Received: 5 August 2024
Revised: 14 September 2024
Accepted: 18 September 2024
Published: 20 September 2024

1. Introduction

"Urban air mobility" (UAM) is an advanced air transportation system for passengers and cargo, in and around densely populated areas and urban environments [1]. By moving part of the "transport network" into the air, the UAM market aims to substantially reduce the amount of traffic congestion in highly populated cities, decrease local CO_2 emissions, and ensure much faster and safer mobility: direct routes would save up to 70% of the average travel time in a standard city, and the interconnection between vehicles would ease fleet management and reduce the risk of fatal accidents [2]. Vertical take-off and landing (VTOL) capabilities and sustainability are the main requirements for aircraft operating in a UAM ecosystem: different configurations of electric and hybrid VTOL have been developed to satisfy the typical mission requirements of range, endurance, and speed in urban scenarios [3]. Indeed, the majority of current research efforts are concentrated on creating novel VTOL designs that can be employed for various purposes. For example, a performance study of three concept vehicles for air taxi operations was presented by Johnson et al. [4]: a fifteen-passenger tilt-wing with turbo-electric propulsion, a six-passenger side-by-side helicopter with hybrid propulsion, and a single-passenger electric drone in a quadrotor layout were compared using their ideal mission scenarios. Due to its limited endurance and ability to operate in constrained regions, the multirotor drone performed best in short-range applications. In medium-range missions, the hybrid-powered side-by-side helicopter ensured maximum performance, while a turbo-electric propulsion system

was still required to maximize the range. In the latter instance, compared to the other designs, the tilt-wing approach offered significantly higher cruising efficiency. For the aim of reducing local CO_2 emissions, sustainable propulsion systems must be exploited. The opportunity to fly with unmanned systems (UASs) is an additional milestone that the UAM market is attempting to achieve. Operating with fully autonomous vehicles may provide advantages in the management of a large number of UASs, together with route optimization and reductions in costs [5]. The interconnection between vehicles would guarantee safety and fast decision-making in emergency situations, as well as improvements in air traffic control. For this purpose, Mathur et al. [6] proposed two reference paths for industries and international agencies to accelerate the transition towards UAM. In their work, the authors highlighted the key challenges to be addressed before unmanned systems can be introduced in a UAM ecosystem and how current systems must evolve. Indeed, while from a regulatory point of view, the European Aviation Safety Agency (EASA) is still working to guarantee solid and efficient rules, from a technological and performance standpoint, several studies have already been carried out. For instance, Zong et al. [7] investigated the feasibility of hybrid and electric propulsion systems on small UAVs (unmanned aerial vehicles), highlighting the benefits of series/parallel hybrid layouts and mission profile performance. Because of the limited endurance and range of all-electric configurations with current battery technology, these technologies have still not been widely adopted. At a larger scale, Bacchini and Cestino [8] carried out an analytical investigation of the speed and endurance of commercial eVTOLs. They calculated the mission performance of the lift + cruise Kitty Hawk Cora, the vectored thrust Lilium Jet [9], and the coaxial drone E-Hang 184 [10]. They found that a multirotor drone is the best option for hovering conditions, while a vectored thrust ensures greater speed and range. The lift + cruise approach might be regarded as the best option for mixed, medium-range missions, since it strikes a balance between cruising and hovering capabilities. However, the idea of employing classical and well-known configurations such as single-rotor helicopters is another option.

In general, the process of selecting the absolute best configuration for a specific mission is still an open question, since a precise methodology for comparing equivalent rotorcraft and UAVs has not been defined. While it was observed from the literature that each viable configuration presents the optimal performance in different mission scenarios, it is still not clear how multiple layouts carrying different payloads and with alternative propulsion systems can be compared with each other to define the absolute best in terms of performance in a reference mission. The present paper aimed to compare three different VTOL configurations, developed in a conceptual design by starting from a classical single-rotor helicopter. The original contribution to the scientific community is connected to the methodology adopted: a reference rotorcraft design is taken as a starting point to design comparable alternative configurations, having similar structure, payload, weight, and propulsion system. For this aim, a 760 kg lightweight, turbine-powered, helicopter was ideally electrified to fulfill the sustainability requirement, and an analytical framework for the evaluation of the performance of general eVTOLs is presented. In particular, a side-by-side helicopter was designed together with a 6-rotor drone (hexacopter). The same unique methodology was applied in all the cases, making the results reliable and comparable. A methodology for designing battery packs and scaled electrical powertrains was proposed and applied to the case studied. This paper continues with additional considerations on the societal acceptance, safety, and theoretical noise emissions regarding each of the analyzed cases.

2. Materials and Methods

2.1. Mathematical Modeling

The mathematical framework to compute the power required by the rotorcraft in different flight conditions is given here. The analytical model was an extension of the work by Avanzini et al. [11], which was based on general momentum and blade element theories. The implementation was first validated with Avanzini's results on a small-scale helicopter

and then extended for the purposes of this work. The model was suitably modified to take into account multiple rotors and vertical flight conditions, neglecting the aerodynamic interactions between the rotors and assuming each of them works separately. The analytical framework was compared and validated with the results of [4] for an analysis of multiple-rotor configurations. The power balance equation defines the total power required by the shaft in steady flight conditions as

$$P_{sh} = \frac{P_p + N_r P_{mr}}{\eta_{mr}} + \frac{P_{tr}}{\eta_{tr}} + P_s \tag{1}$$

where P_s and P_p are the power required by the auxiliary systems and parasite power due to fuselage drag, respectively, while η_{mr} and η_{tr} are the main and tail rotor transmission efficiencies (assumed to be constant). P_{mr} and P_{tr} are the power required by the main and tail rotor as reported by Avanzini [11]. The total thrust needed to sustain the rotorcraft is distributed along N_r contributions, where N_r is the number of main rotors. Considering a T_i thrust force provided by a single main rotor,

$$T_i = \sqrt{\left(\frac{W}{N_r}\right)^2 + \left(\frac{D}{N_r}\right)^2} \tag{2}$$

where W and D are the total weight and fuselage drag forces in a simplified two-dimensional representation. D depends on an equivalent flat plate parasitic area f, such that $D = \frac{1}{2}\rho f U^2$ (U is the true airspeed and ρ the air density) and the parasite power is

$$P_p = \frac{1}{2}\rho f U^3 \,. \tag{3}$$

The power required by the main rotor is provided by the sum of the induced and profile power contributions, respectively,

$$P_{ind} = N_r k_{ind} T_i v_i \tag{4}$$

$$P_{pr} = N_r \rho A (\Omega R)^3 C_{p_{pr}} \tag{5}$$

where v_i is the induced inflow velocity derived from momentum theory [12], Ω is the rotor angular speed, and $C_{p_{pr}}$ is the profile power coefficient [11]. The induced power factor k_{ind} is the momentum-theory-defined ratio of the induced to the ideal power. This factor accounts for several aerodynamic losses, including non-uniform inflow and blade tip losses. In an experimental investigation, Nabawy et al. [13,14] estimated k_{ind} for the wings of various insects, demonstrating its dependence on the thrust coefficient, linear twist, and number of blades. However, because of the lack of experimental data for rotorcraft, and for the sake of simplicity, k_{ind} is held constant in this analysis and set to 1.25.

A substantial difference occurs between helicopter, side-by-side, and multirotor configurations. Indeed, while both side-by-side and classical helicopters work at constant rotor angular speed and the same modeling approach can be adopted for both configurations, a multirotor works with variable RPM control and fixed blade pitch, meaning that the rotor's angular speed depends on the flight condition. P_{pr} directly depends on Ω, both in the equation and the profile power coefficient. For a preliminary performance analysis of a multirotor, Ω can be determined by the experimental thrust–RPM curve provided by commercial electric motors coupled with high-performance propellers. For the sake of this study, a reference motor + propeller system was adopted [15], and the RPM as a function of the required thrust was extrapolated from specifications. Similarly to the side-by-side helicopter case, the total thrust was distributed between the single rotors, each of them rotating at the specific RPM derived from its characteristic curve. In addition, for the helicopter configuration ($N_r = 1$), the tail rotor contribution to total power was added in the expression. The tail rotor was modeled analogously with the main rotor, with the

required thrust defined by the flight condition and the distance between the two rotors, to balance the external moment. In particular,

$$T_{tr} = \frac{P_p + P_{mr}}{\Omega} \frac{1}{l_{tr}} . \tag{6}$$

In vertical flight conditions, the model accounts for the incoming flow occurring in steady climbing and vertical descending. The parasitic power is evaluated as

$$P_p = D_v |U_v| = \frac{1}{2} \rho f_v U_v^2 |U_v| \tag{7}$$

where U_v is the climbing/descending speed and f_v is the equivalent parasitic flat plate area in the vertical direction. The contribution of the induced speed v_i to the vertical drag was disregarded for the sake of simplicity. The air density in vertical flight was averaged between the initial and final altitudes of the constant vertical motion. Since the induced velocity v_i must account for the vertical speed, the induced power P_{ind} was also adjusted for vertical flight. Specifically, the induced speed inside wake, vortex, and windmill brake regions for both climbing and descending were estimated using the semi-analytical model created by Johnson [16] and

$$P_{ind} = k_{ind} T_i (U_v + v_i) \tag{8}$$

2.2. Configuration Design

Three different conceptual designs were developed by starting from a reference airframe. In particular, a turbine-powered lightweight helicopter with a maximum take-off mass equal to 760 kg represented the starting setup [17]. The vehicle was ideally electrified by removing all components related to the turbine engine and replacing them with an electric motor and a battery. Two alternative UAS configurations with rotating blades were considered: a side-by-side helicopter, and a hexacopter drone (Figure 1).

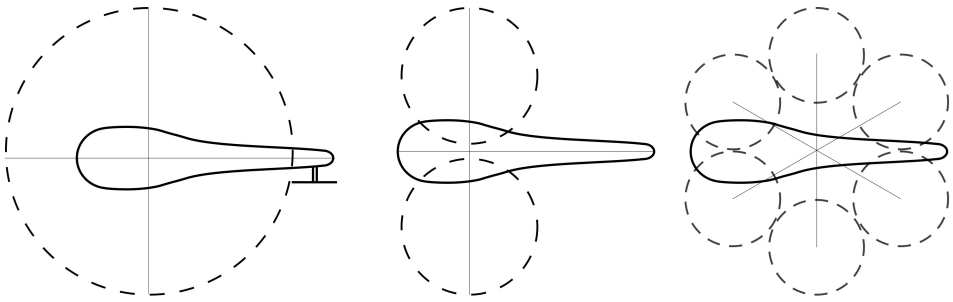

Figure 1. Rotorcraft conceptual design scheme.

The same fuselage and empty mass ratio of the original layout were kept, in order to compare the performance of multiple rotors and different operating systems (constant and variable RPM) within the same framework. The requirements for the conceptual design were:

- a maximum take-off mass of 760 kg;
- two passenger payload (175 kg);
- the maximum size of the rotorcraft not exceeding 7.6 m;
- battery discharge limit of $SoC = 30\%$;
- max. hovering throttle at 500 m: 65%;
- objective endurance: 50 min;
- the same structure and fuselage;

The latter, in particular, was a general approximation made to be able to compare the performance of the rotorcraft, as they would be designed in an equivalent way. Adopting the same fuselage for the three conceptual models provided the same aerodynamic loads and a constant weight and volumes. The helicopter design was provided by de

Angelis et al. [17], while the side-by-side and drone were designed accordingly. For the first aircraft, the rotors were designed from the required maximum width, and the rotor angular speed was derived by keeping the same blade tip speed as the single-rotor configuration. The rotor blades maintained the same aspect ratio and a constant airfoil along their span. A similar approach was applied to the multirotor, but with the inclusion of the analyzed propeller [15], which had variable RPM. For the sake of this study, a hexacopter was considered, as the more classical quadrotor brings some criticalities in safety and residual controllability. In particular, while the constant-RPM machines (helicopter and side-by-side) can rely on the autorotation maneuver in case of engine failure [18], drones implement safety measures through the redundancy of their rotors. Indeed, residual controllability of the system in case of one rotor failure is only guaranteed with systems having a minimum of six rotors, while in the case of a two-rotor failure, only if these two are not adjacent. For this reason, the quadrotor configuration was neglected a priori in this study and a hexacopter layout was considered representative of the multirotor category. The helicopter's blades were scaled to estimate the single-blade mass of different VTOLs as

$$m_b = \frac{m_{b_0}}{R_0} R \tag{9}$$

where the subscript $_0$ refers to the helicopter's original design. Finally, while for the hexacopter, the selected motor was already defined by the coupled motor + propeller system in the references, a scaled set of N_r electric motors were selected for the single and dual rotor layout. In particular, linear scaling was applied by considering the set of commercial motors produced by EMRAX (Kamnik, Slovenia) [19] (Figure 2). The latter are a family of electric motors properly designed for aeronautical and high-power-density applications. Their relatively low weight and high-power characteristics make this family of propulsion systems an excellent candidate to sustain UAM vehicles and perform advanced air mobility services. An extensive discussion on the properties of EMRAX products in comparison with similar motor designs was conducted by Ivanov et al. [20]. In addition, the various motor sizes designed with the same technology, and the availability of their technical datasets [21], make this product very suitable for analytical scaling, as proposed in this work. The scaled motors were selected by fixing the required maximum power for a hovering throttle of 65% at 500 m altitude and computing the equivalent weight with a second-order polynomial interpolation of the commercial models. A similar approach was applied for the derivation of the specific load factor and the equivalent power/RPM curves. The final rotorcraft design specifications are summarized in Table 1.

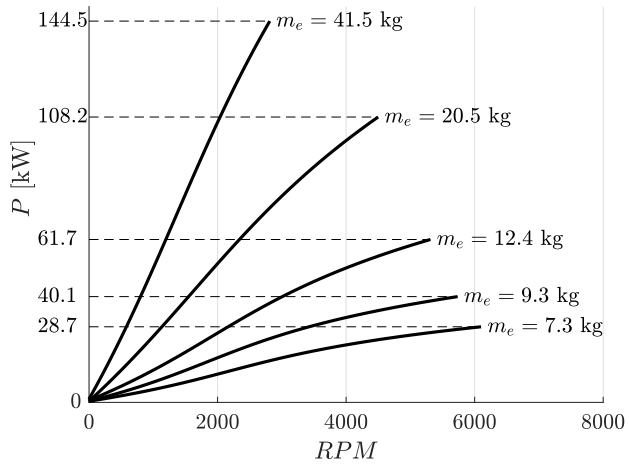

Figure 2. EMRAX motor scaling curves.

Table 1. Rotorcraft conceptual design specifications.

			Helicopter	**Side-by-Side**	**Hexacopter**
Max. take-off mass	$MTOM$	[kg]	760	760	760
Empty mass	m_0	[kg]	301.2	299.4	306.3
Payload mass	m_p	[kg]	175	175	175
Motor mass	m_e	[kg]	74.4	23.1	11
Battery mass	m_b	[kg]	209.4	239.4	212.7
Electric motor					
Type			Scaled	Scaled	Commercial
Number of motors	N_r		1	2	6
Maximum motor power	P_{max}	[kw]	183.5	110.8	45
Specific load factor	sls	[RPM/Vdc]	1.22	6.08	16.4
Main Rotor					
Eq. flat plate area	f	[m^2]	2.137	2.137	2.137
Number of blades	N_b	-	2	2	2
Rotor radius	R	[m]	3.8	1.9	0.8
Chord	c	[m]	0.195	0.098	0.08
Solidity ratio	σ	-	0.033	0.033	0.0637
Angular velocity	Ω	[RPM]	528.5	1057	-
Disk loading	DL	[kg/m^2]	16.8	25.8	48.5
Blade's drag coeff.	C_{d_0}, k	-	0.008, 0.008	0.008, 0.008	0.008, 0.008
Tail Rotor					
Rotor radius	R_t	[m]	0.57	-	-
Chord	c_t	[m]	0.12	-	-
Solidity ratio	σ_t	-	0.038	-	-
Angular velocity	Ω_t	[RPM]	3061	-	-
Blade's drag coeff.	$C_{d_{0_t}}, k_t$	-	0.008, 0.008	-	-

2.3. Battery Design

The battery pack design methodology is described in this chapter. A series and parallel arrangement of single cells maximized the total capacity of each battery, while adhering to the maximum take-off mass ($MTOM$) requirement and matching the motor's voltage in the hovering situation. Figure 3 depicts a typical battery pack arrangement. The design methodology necessitated an iterative process, as every time the total number of cells changed, the overall $MTOW$ of the system varied accordingly, and with it the electric motor voltage which depends on the power demand in hovering conditions. It is worth mentioning that, when a group of cells are connected in series, the total voltage that is achieved for the battery pack is the total of the individual cell voltages. Conversely, when a group of cells are arranged in parallel, the voltage stays constant, but the total capacity is the sum of the capacities of each cell series. In this manner, a series cell arrangement can produce the necessary nominal voltage, and a parallel cell arrangement can maximize capacity. An explanation of the methodology is given in Figure 4.

The algorithm looked for the best combination of n_{cs} and n_{cp} (number of cells arranged in series and parallel, respectively) to match the nominal voltage of the battery (V^b_{nom}) with that of the motor (V^e_{nom}) to maintain the rotorcraft in a hover. The characteristic power curve of the electric machine links the power required at the shaft P_{sh} and the rotational frequency of the motor RPM. An electrical motor's specific load speed sls is a metric that links voltage and frequency. At each iteration, the number of cells in series and parallel is computed as

$$n_{cs} = round\left(\frac{V_{nom}^{e}}{V_{nom}^{c}}\right) \tag{10}$$

$$n_{cp}^{new} = n_{cp}^{old}\, floor\left(\frac{MTOW_{max} - MTOW(n_{cs}^{new}, n_{cp}^{old})}{n_{cs} m_c}\right) \tag{11}$$

where $MTOW_{max}$ is the maximum allowed total weight, m_c is the mass of a single cell, and $MTOW(n_{cs}^{new}, n_{cp}^{old})$ is the total mass computed with a battery having the new n_{cs} and the n_{cp} computed in the previous iteration. In this sense, the n_{cs} tends to match the nominal voltages, while n_{cp} is used to fill up the remaining available mass and maximize the capacity, and thus the endurance. Indeed, the endurance in ideal discharge conditions is

$$t_{id} = \frac{C_0 V_{nom}}{P_{sh}} \eta_e \tag{12}$$

where η_e is the electrical efficiency of the system. At every iteration, the mass of the rotorcraft is updated with the "new" battery cell arrangement, which defines the battery mass as $m_b = n_{ns} n_{cp} m_c$; its nominal voltage (V_{nom}^{b}); and nominal capacity (C_0^{b}). In the equation shown in Figure 4, the "empty mass" m_0 is defined as the mass of the rotorcraft without a payload or electric propulsion system, while the mass occupied by the motors is $N_e m_e$ (where N_e and m_e are, respectively, the number and mass of the single motors), and m_p is the payload. The algorithm stops when both the requirements for voltage error and variation in the number of series cells are achieved. Indeed, the stopping criteria are

$$V_{nom}^{err} = \frac{|V_{nom}^{e} - V_{nom}^{b}|}{V_{nom}^{e}} < tolerance \tag{13}$$

and

$$dn_{cs} = n_{cs}^{new} - n_{cs}^{old} = 0 \tag{14}$$

The silicon anode battery (Si-A) cells produced by Amprius (Fremont, CA, USA) [22] were selected for this paper because they offer a better energy density than traditional lithium ion (Li-Ion) batteries, . This technology guarantees the maximum energy density currently available on the market, with an acceptable limit regarding the maximum discharge rate exploitable from the pack. Further descriptions of Amprius batteries and silicon anode technology can be referred to in the works of Feng [23] and Tang [24]. Table 2 reports the battery cell details.

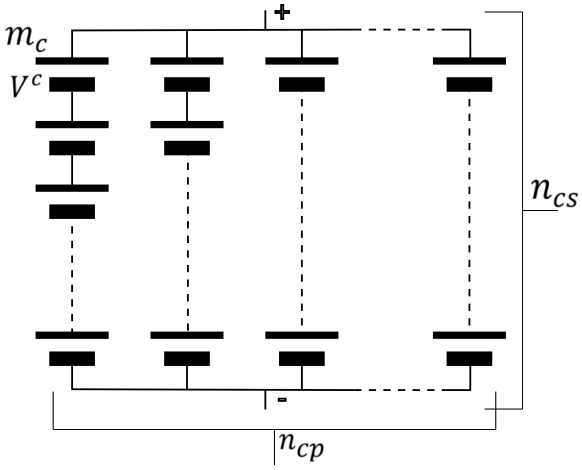

Figure 3. Battery pack configuration.

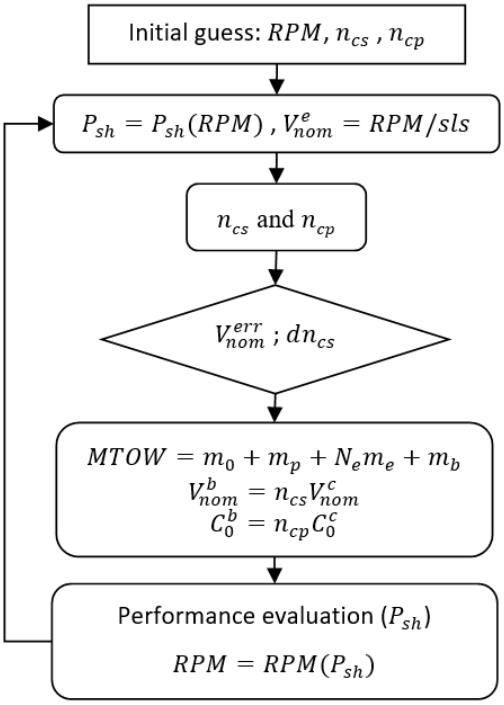

Figure 4. Battery design iterative procedure.

Table 2. Battery cell parameters.

Battery Type: Silicon Anode (Amprius Technologies [22])		
Nominal voltage	V_{nom}^{c}	3.7 V
Nominal capacity	C_0^{c}	3.8 Ah
Max. discharge rate	C_{rate}	3 C
Energy density	E_d	425 Wh/kg
Cell mass	m_c	33 g

2.4. Battery Discharge Model

A constant-power battery discharge model was proposed in this work to estimate the endurance of the rotorcraft batteries. For this work, an analytical framework was extrapolated from the experimental study conducted by Avanzini et al. [25]. In their work, a series of tests on Li-Po batteries were carried out to determine the overall duration t, depending on the battery capacity C, the number of cells N, and the constant discharge power P_b. An exponential model was implemented as

$$t = \alpha(N, P_b) C^{\beta} \tag{15}$$

where α is a function of the power and the number of cells. The values of α were obtained in experiments for variables P_b and N and interpolated by applying a variable separation method. Nevertheless, the interpolation adopted by Avanzini has the criticality of diverging when the number of cells increases and it could not be applied in this paper. As such, an alternative interpolation method was applied:

$$\alpha(N, P_b) = a(N) P_b^{b(N)} + c(N) \tag{16}$$

where

$$\begin{cases} a(N) & = 4.129N - 0.2241 \\ b(N) & = -1.003 \\ c(N) & = -0.03244 N^{-1.43} + 3.161 \cdot 10^{-4} \end{cases} \tag{17}$$

so $a(N)$, $b(N)$, and $c(N)$ are, respectively, linear, constant, and exponential functions of N. In order to scale the results to the Si-A batteries employed in this paper, a simple linear proportion was performed using the nominal voltage of the cells, to the experimental values of α, namely α_{exp}, such that

$$\alpha = \alpha_{exp} \frac{V^c_{nom}(\text{Si} - \text{A})}{V^c_{nom}(\text{Li} - \text{Po})} \quad . \tag{18}$$

The experimental data are reported in Figure 5.

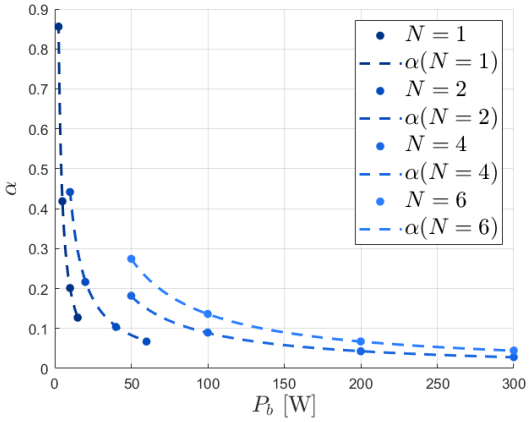

Figure 5. Experimental α values and small N interpolation.

2.5. Mission Design

The VTOLs and drone performances were evaluated in a reference mission. Table 3 describes the mission profile.

Table 3. Mission design.

	Altitude	**Speed**	**Time**
Climb	$0 \rightarrow 500$ m	$U_v = 4$ m/s	2.08′
Hover	500 m	-	2.00′
Cruise	500 m	U_{BSE}	T_c
Hover	500 m	-	2.00′
Descent	$500 \rightarrow 0$ m	$U_v = -4$ m/s	2.08′

The mission had a total duration of T_{tot} in the best specific endurance condition. The cruising phase T_c was maximized to complete the flight without falling below the discharge limit (Section 2.2). As a general rule of thumb, normal batteries cannot be discharged below a certain limit without damage, thus a fixed minimum state of charge (SoC) of 20% was set.

3. Results

The performance of the three rotorcraft configurations was studied in terms of the power required, maximum endurance, range, and performance in the reference mission. The methodology described in Section 2.3 was applied for the three cases to produce the battery pack designs reported in Table 4. Considering the design requirements, the battery pack was designed to maximize the capacity, while matching the electric motor nominal voltage at 65% of its maximum power. The available space in each vehicle was different, since different compressive motor weights were produced; therefore, the side-by-side helicopter was reported to be the rotorcraft with the highest energy carried onboard. Similar battery packs were produced for the helicopter and the multirotor, with a different cell arrangement.

Table 4. Battery design.

			Helicopter	Side-by-Side	Hexacopter
Pack design	$n_{ncs} \times n_{cp}$	[-]	171 × 37	113 × 64	102 × 63
Battery mass	m_b	[kg]	209.4	239.4	212.7
Nominal voltage	V^b_{nom}	[v]	632.7	418.1	377.4
Nominal capacity	C_0	[Ah]	140.6	243.2	239.4
Ideal energy	E	[kwh]	89.0	101.7	90.4

The power curves for each configuration are reported in Figure 6. On the vertical axis, the total shaft power computed with Equation (1) at different forward speeds is reported. As mentioned in the equation, the power required in each flight condition was the sum of different contributions, namely the induced, rotor profile, and parasite powers. The plot provides the envelope of power curves from an empty ($m_p = 0$ kg) to a maximum load condition, showing the variation in power for the different payloads. Different considerations can be taken from this plot. In general, the multirotor design was the highest-power-consuming configuration, with a hovering power in a fully loaded layout of 180.2 kW. The dual-rotor configuration was a compromise between the others, requiring 140.9 kW to keep a steady hovering condition, while the helicopter's hovering power was 117.5 kW. Considering low-speed conditions (below the minimum power speed), the helicopter was the most efficient configuration, as it required a minimum power to hover and perform forward flight in both empty and fully loaded layouts. Low-speed regimes are governed by the induced power, which is directly proportional to the disk loading, defined as the ratio between the thrust and the rotor-swept area. A larger disk loading leads to a low power efficiency at low speeds. At flight regimes above the minimum power, the slopes of the side-by-side and helicopter curves merged until the first became lower. It is known, indeed, that single-rotor layouts are suitable for low-speed operations, while a larger number of rotors brings advantages at higher speeds [26].

The plots also highlight the power sensibility to weight variation of each configuration. Indeed, the envelope of the multirotor had a larger span with respect to the others, indicating large power variations with variable loads. This effect is generally linked to two factors: the subdivision of the lifting surface, and hence the increase in disk loading in a multirotor machine; and the lower efficiency of the variable RPM system. The latter represents an important criticality of this system, since the propeller design can be optimized to only operate in a specific flight condition and becomes highly inefficient as soon as the rotorcraft changes speed or payload. However, with this effect connected to the variation in the induced power factor, which was, for the sake of simplicity, kept constant and equal for the three configurations, the evaluation of this phenomenon fell outside of the scope of this paper, and the power jump highlighted in this Figure is mostly related to the disk loading effect. In general, from a power-required point of view, the more classical single-rotor configuration remains the best choice for an efficient UAM service operating with rotary wing layouts. The parameter ΔP_h was adopted to highlight the power jump between a fully loaded and an empty configuration in hover, and decreased as the disk loading decreased.

Rotorcraft performance was also evaluated by means of their theoretical maximum endurance and range. By applying the battery discharge model described in Section 2.4 at different forward speeds, the maximum endurance and range achievable by each rotorcraft were computed and are reported in Figure 7. While for the best specific endurance (subscript $_{BSE}$) condition, the helicopter was undoubtedly the best configuration, from a maximum range perspective, the side-by-side and helicopter achieved similar results. The main design features and performance are summarized in Table 5. The multirotor design described in this work had the main advantage of reducing the overall maximum width of the configuration, but on the other hand, achieved the highest disk loading. The latter affected the required power at low speed, leading to a very limited maximum endurance and a low mass-to-power ratio when hovering.

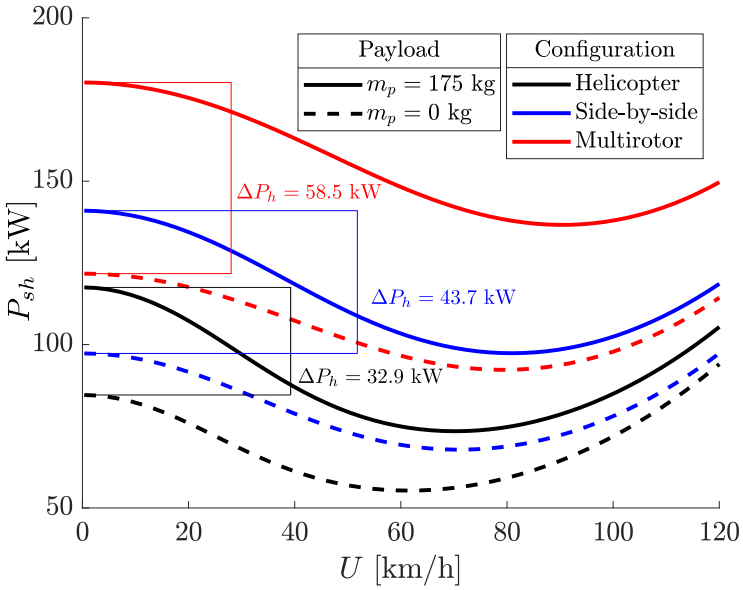

Figure 6. Power curves in a fully loaded and empty configuration.

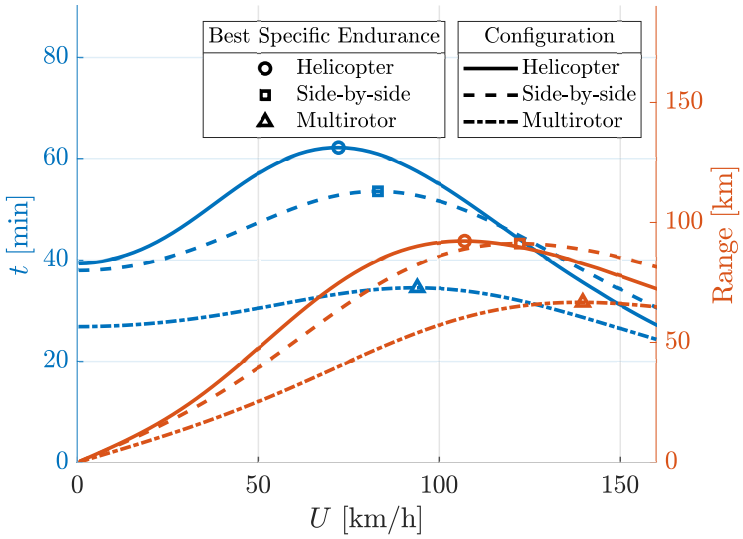

Figure 7. Best specific endurance and range.

Table 5. Rotorcraft performance.

			Helicopter	Side-by-Side	Multirotor
Number of rotors	N_r	[-]	1	2	6
Max. take-off mass	$MTOM$	[kg]	760	760	760
Max. width	$L(R)$	[m]	7.6 (3.8)	7.6 (1.9)	4.8 (0.8)
Disk loading	DL	[kg/m^2]	16.8	33.5	62.9
Hovering power	P_h	[kw]	117.5	140.9	180.2
Hovering power ratio	$P_h/(N_r P_{max})$		64 %	64 %	67 %
Hovering efficiency	$MTOW/P_h$	[N/kW]	6.5	5.4	4.2
Best specific endurance	P_{BSE}	[kw]	74.1	99.4	141.7
	T_{BSE}	[min]	62.1	53.5	34.5
	U_{BSE}	[km/h]	72.2	83.1	94.0
Best specific range	P_{BSR}	[kw]	89.6	120.5	174.2
	X_{BSR}	[km]	92.2	91.2	66.7
	U_{BSR}	[km/h]	107.1	122.3	139.8

It should be highlighted that the maximum endurance and range described in Figure 7 consider a rotorcraft operating at a constant speed and consuming the maximum available energy. However, in a realistic scenario, vertical flight and hovering phases must be considered. Figure 8 represents the battery state of charge (SoC) during the UAM mission designed in Section 2.5 for the three cases. The mission included a first climbing phase to reach the cruising altitude of 500 m, 2 min of hovering, a cruising phase at the best specific endurance speed (U_{BSE}), and final hovering and descending phases to reach the ground with the minimum level of SoC. The battery energy constantly decreased with a quasi-linear trend during the different phases of the mission. The higher the power demand, the higher the rate of discharge, and thus the steeper slope in that range. It is worth mentioning that the constant–power discharge model provided an approximate rate of discharge, which was not perfectly linear and was, indeed, more conservative than the typical ideal case. The single-rotor VTOL was the aircraft that achieved the maximum endurance during the mission, followed by the side-by-side and the multirotor. Concerning the achieved range, the helicopter and side-by-side achieved similar values. Indeed, while the first was more suitable for low speed operations, the second configuration achieved a higher best specific endurance speed. The multirotor had the worst performance in the analysis and very limited endurance capabilities. The mission results are reported in Table 6. It is highlighted that all the designs satisfied the maximum discharge rate limit of 3C imposed by Si-A technology for the entire duration of the mission.

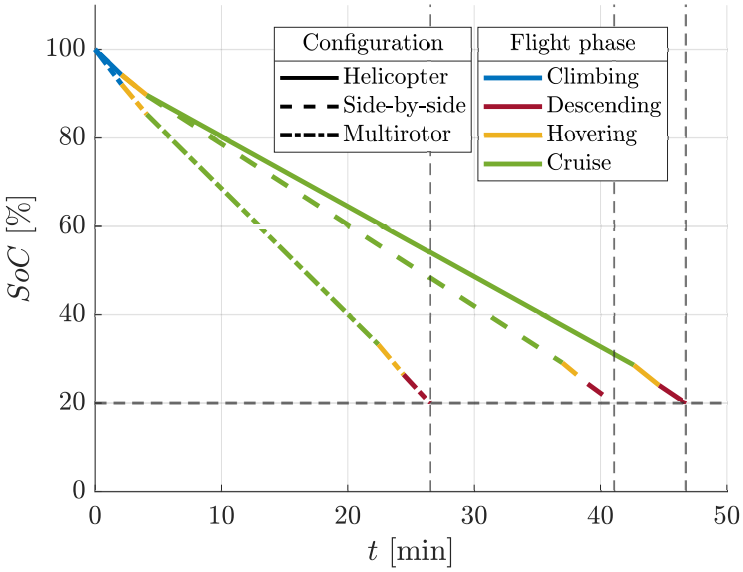

Figure 8. Mission SoC.

Table 6. Mission results.

			Helicopter	Side-by-Side	Multirotor
Discharge rate in hover	C_{rate_h}	[C]	1.32	1.39	1.99
Discharge rate in cruise	$C_{rate_{BSE}}$	[C]	0.83	0.98	1.57
Discharge rate in climbing	$C_{rate_{cli}}$	[C]	1.60	1.62	2.30
Discharge rate in descending	$C_{rate_{des}}$	[C]	1.11	1.21	1.85
Total mission duration	T_{tot}	[min]	47	41	26
Cruising time	T_c	[min]	39	33	18
Range	X_{tot}	[km]	46.4	45.6	28.7

4. Discussion

From a performance analysis point of view, the single-rotor helicopter configuration provided the minimum power demand in most of the analyzed flight phases and had

the theoretical best endurance and range. However, when selecting the most suitable configuration for UAM services, several additional factors must be considered.

The first fundamental aspect is the confidence that a UAM ecosystem generates in its direct users. An extensive analysis of the societal acceptance of UAM operations was conducted by the European Aviation Safety Agency (EASA) in 2021 [27]. The study performed surveys and interviews about the major concerns and expectations of European citizens concerning UAM: a generally positive attitude was observed, as it was seen as a viable solution to reduce travel time, traffic jams, and urban pollution. On the other hand, safety and security were the major concerns, together with noise and environmental impacts. To this extent, the three configurations considered in this study present different characteristics.

As already mentioned in Section 2.2, the constant RPM and variable collective pitch system adopted by helicopters and, theoretically, by a side-by-side configuration, guarantee the capability of performing an autorotation maneuver in case of propulsion system failure [18]. An additional level of safety can be introduced in the side-by-side configuration by operating the two rotors semi-autonomously, with each of them driven by a specific electric motor connected to the other with a drive belt. This redundancy guarantees that, when one of the two motors fails, the other can drive both of them to a safe landing. The multirotor analyzed in this paper, instead, guaranteed residual controllability in case of failure of one or two non-adjacent rotors.

Safety and societal acceptance could also be improved by implementing shrouded rotors [28]. The design of ducts protecting and isolating the rotors would be a fundamental requirement for UAVs operating in a UAM ecosystem. The latter would avoid the presence of open rotors and even improve blade aerodynamic efficiency, at the cost of an increased take-off mass [12]. Indeed, the presence of rotating blades near future passengers is of major concern for the safety of both the professional and nonprofessional public. Safety procedures for boarding and disembarking would be fundamental to avoid collision with rotating propellers and dangers related to the inflow velocity produced by the rotors. However, while this solution is not practical on classical helicopters with a single main rotor, and with a difficult implementation in multirotors, side-by-side configurations can provide a perfect fit with this measure. An example of a side-by-side helicopter with ducted fans was proposed by SAB s.r.l. in a small-scale prototype [29].

Noise level is another area of concern for UAM users. The aerodynamic interactions between multiple rotors and between rotors and fuselage may generate noise levels that are outside the limits imposed by urban transport regulations [30]. Consider, for example, the case of side-by-side helicopters with intermeshing rotors: it was found by Sagaga et al. [31] that the amount of noise emitted by a rotorcraft was directly affected by the level of overlap between the rotors and can be reduced by increasing their distance. On the other hand, the rotor–fuselage interaction [32,33] is strictly inevitable in a classical single-rotor configuration, while it can be avoided in multiple-rotor UAVs. The latter solution would increase the total width of the rotorcraft but avoid the impact between the fuselage and the rotor inflow. The acoustic footprints generated by single or multiple rotors can be evaluated by adopting analytical [34], numerical [35], or experimental methods [36]. Smith et al. [37], for example, compared multirotor noise characteristics with an increasing number of rotors and variable disc loading. A general observation was that, for higher disk loadings, the overall noise levels increased significantly. The latter led to conclusions about the optimal number of rotors for minimizing acoustic levels. Considering a constant maximum take-off weight and a fixed maximum width, operating with a single, larger main rotor would be beneficial for the overall noise produced by a VTOL. Multirotor and side-by-side configurations generally have higher disk loadings than helicopters [38], requiring a higher power during low-speed flight phases and producing more noise. In general, the overall noise produced by a specific VTOL depends on several factors, such as the number of rotors and their rotational speed, the fuselage design, the presence of ducts, and the relative location, and thus interaction, of the rotors. A unique solution to which of the three analyzed cases would produce the highest noise disturbance cannot be found at a

conceptual design stage and requires advanced investigations of more realistic designs. However, if neglecting the aerodynamic interactions between rotors and fuselage, and the tail rotor contribution, it can be concluded that a single-rotor design could provide lower disturbances to citizens and users with respect to multiple rotors restricted to the same width.

5. Conclusions

In the present study, a performance analysis of multiple VTOL configurations was carried out using an analytical representation. Starting from an initial turbine-powered helicopter with a maximum take-off mass of 760 kg, three different eVTOL configurations were proposed and designed at a conceptual stage: a classical helicopter, a side-by-side dual-rotor machine, and a six-rotor drone. The paper exploited an innovative electrification and design methodology for full-electric rotorcraft, including a battery pack design coupled with a scaled electric motor and requirements for the definition of the main rotorcraft parameters. With respect to similar literature studies, the paper managed to design alternative configurations starting from a standard layout. The adopted method made the conceptual solutions comparable in a reference mission profile and allowed defining the optimal technology from a performance perspective. An analytical model for estimating the rotorcraft performance in terms of power demand, endurance, and range was presented for both constant and variable RPM systems, and a semi-analytical battery-discharge model was included in the formulation. A reference mission was designed to test the different configurations in a realistic UAM scenario. The mission included five flight phases, starting with an initial climb to the cruising altitude, hovering, cruise, and a final descent to the ground.

The performance of the three configurations was studied, and the main outcomes are summarized as follows:

- three conceptual designs with a fixed maximum take-off mass were produced, and a specific battery pack plus electric motor configuration was provided for each of them;
- the helicopter was revealed to be the lowest-power-demanding configuration at low speed and the most efficient in both the full and empty payload layouts. On the other hand, the multirotor with a variable RPM system turned out to be highly inefficient as soon as its design was not optimized for a specific flight phase, indeed the power jump between fully loaded and unloaded layouts was the highest;
- from a maximum endurance and range perspective, the helicopter and side-by-side achieved the best performance, with the former standing out for its best specific endurance;
- in the reference mission profile, the helicopter achieved 46 min of flight, including initial and final vertical flight and hovering phases, against the 41 min of the side-by-side and the 26 min of the multirotor.

From a performance perspective, the classical single-rotor VTOL configuration is undoubtedly the best for performing short-range flights and to incorporate a fully electric propulsion system. However, additional considerations must be made regarding fundamental aspects of the inclusion of a UAV into a UAM ecosystem. Such aspects include societal acceptance, safety, and noise emissions. According to the discussion, the side-by-side helicopter stood out as a promising candidate from these perspectives, even if an advanced quantitative study is required. In conclusion, the classical single-rotor helicopter achieved the best performance in terms of power demand, endurance, range, and mission duration, but may present some criticalities in terms of safety, societal acceptance, and noise disturbances due to the aerodynamic interactions between the rotor and fuselage. From a design point of view, the side-by-side helicopter represents a trade-off between classical helicopters and multirotors, merging the better performance of a constant RPM system with the design simplicity of a symmetric machine. Safety and security were the main user concerns about VTOLs, and the side-by-side helicopter satisfies both redundancy requirements and the capability to perform emergency maneuvers in case of failure. Ducted rotors improve safety for external users and increase the level of societal acceptance by

covering the rotating blades. From a noise level point of view, this configuration is theoretically less efficient than a classical helicopter, but its performance should be re-evaluated by considering the low level of aerodynamic interactions occurring by placing the main rotors outside of the fuselage boundaries.

Author Contributions: Conceptualization, E.L.d.A., F.G., A.T. and F.L.; methodology, F.M., E.L.d.A. and F.G.; software, F.M.; validation, F.M.; formal analysis, F.M.; investigation, F.M.; resources, E.L.d.A., F.G., A.T. and F.L.; data curation, F.M.; writing—original draft preparation, F.M.; writing—review and editing, F.M., E.L.d.A., F.G. and A.T.; visualization, F.M.; supervision, E.L.d.A., F.G. and A.T.; project administration, F.L. and A.T.; funding acquisition, E.L.d.A., F.G., A.T. and F.L.; All authors have read and agreed to the published version of the manuscript.

Funding: This study was carried out at MOST—Sustainable Mobility National Research Center and received funding from the European Union Next-GenerationEU (PIANO NAZIONALE DI RIPRESA E RESILIENZA (PNRR)—MISSIONE 4 COMPONENTE 2, INVESTIMENTO 1.4—D.D. 1033 17/06/2022, CN00000023). This manuscript only reflects the authors' views and opinions, neither the European Union nor the European Commission can be considered responsible for them.

Data Availability Statement: The raw data supporting the conclusions of this article will be made available by the authors on request.

Conflicts of Interest: The authors declare no conflicts of interest

References

1. Hill, B.P.; DeCarme, D.; Metcalfe, M.; Griffin, C.; Wiggins, S.; Metts, C.; Bastedo, B.; Patterson, M.D.; Mendonca, N.L. *UAM Vision Concept of Operations (ConOps) UAM Maturity Level (UML) 4*; NASA Technical Management, Document ID: 20205011091; NASA: Washington, DC, USA, 2020.
2. Thipphavong, D.P.; Apaza, R.; Barmore, B.; Battiste, V.; Burian, B.; Dao, Q.; Feary, M.; Go, S.; Goodrich, K.H.; Homola, J.; et al. Urban Air Mobility airspace integration concepts and considerations. In Proceedings of the Aviation Technology, Integration, and Operations Conference, Atlanta, GA, USA, 25–29 June 2018.
3. Svorcan, J.; Kovačević, A.; Popović, L.; Simonović, A. Comparative study of piston vs. electric single-seat tandem helicopter. *Int. J. Sustain. Aviat.* **2022**, *8*, 1–14. [CrossRef]
4. Johnson, W.; Silva, C.; Solis, E. Concept vehicles for VTOL air taxi operations. In Proceedings of the AHS Specialists Conference on Aeromechanics Design for Transformative Vertical Flight, San Francisco, CA, USA, 16–19 January 2018.
5. Gillis, D.; Petri, M.; Pratelli, A.; Semanjski, I.; Semanjski, S. Urban Air Mobility: A State of Art Analysis. In Proceedings of the Computational Science and Its Applications—ICCSA, Online, 11 September 2021.
6. Mathur, A.; Panesar, K.; Kim, J.; Atkins, E.; Sarter, N. Paths to Autonomous Vehicle Operations for Urban Air Mobility. In Proceedings of the AIAA Aviation Forum, Dallas, TX, USA, 17–21 June 2019.
7. Zong, J.; Zhu, B.; Hou, Z.; Yang, X.; Zhai, J. Evaluation and comparison of hybrid wing VTOL UAV with four different electric propulsion systems. *Aerospace* **2021**, *8*, 256. [CrossRef]
8. Bacchini, A.; Cestino, E. Electric VTOL configurations comparison. *Aerospace* **2019**, *6*, 26. [CrossRef]
9. Lilium Jet. Available online: https://jet.lilium.com/ (accessed on 31 May 2024).
10. EHang|UAM Passenger Autonomous Aerial Vehicle (AAV). Available online: https://www.ehang.com/ehangaav (accessed on 31 May 2024).
11. Avanzini, G.; de Angelis, E.L.; Giulietti, F. Optimal cruise performance of a conventional helicopter. *J. Aerosp. Eng.* **2022**, *36*, 865–878. [CrossRef]
12. Leishman, G.J. *Principles of Helicopter Aerodynamics*; Cambridge University Press: Cambridge, UK. 2006.
13. Nabawy, M.R.A.; Crowther, W.J. On the quasi-steady aerodynamics of normal hovering flight part I: The induced power factor. *J. R. Soc. Interface* **2014**, *11*, 20131196. [CrossRef] [PubMed]
14. Nabawy, M.R.A.; Crowther, W.J. On the quasi-steady aerodynamics of normal hovering flight part II: Model implementation and evaluation. *J. R. Soc. Interface* **2014**, *11*, 20131197. [CrossRef] [PubMed]
15. UAV VTOL Herlea 200 kg Thrust Motor. Available online: https://www.austars-model.com/ (accessed on 3 June 2024).
16. Johnson, W. *Helicopter Theory*; Courier Corporation: North Chelmsford, MA, USA, 2012.
17. de Angelis, E.L.; Giulietti, F.; Rossetti, G.; Turci, M.; Albertazzi, C. Toward Smart Air Mobility: Control System Design and Experimental Validation for an Unmanned Light Helicopter. *Drones* **2023**, *7*, 288. [CrossRef]
18. Avanzini, G.; de Angelis, E.L.; Fattizzo, D.; Giulietti F. Autorotation design and simulation for a small-scale helicopter. In Proceedings of the 48th European Rotorcraft Forum, Winterthur, Switzerland, 5–9 September 2022.
19. Fomaro, E.; Cardone, M.; D'Agostino, V.; Dannier, A. An Aircraft Hybrid Electric Propulsion Model Experimentally Validated. In Proceedings of the 2024 International Symposium on Power Electronics, Electrical Drives, Automation and Motion (SPEEDAM), Ischia, Italy, 19–21 June 2024; IEEE: Piscataway, NJ, USA, 2024; pp. 1197–1203.

20. Ivanov, N.S.; Zhuravlev, S.V.; Kharkina, O.A.; Zdorova, M.V.; Shirokov, A.A.; Akhunov, M.T.; Sosova, D.D. Electric Machines with High Specific Power. *Russ. Electr. Eng.* **2023**, *93*, 621–630. [CrossRef]
21. EMRAX | Axial Flux e-Motors | Lightweight | Powerful-EMRAX. Available online: https://emrax.com/ (accessed on 31 May 2024).
22. Amprius Technologies Silicon Anode Batteries. Available online: https://amprius.com/ (accessed on 31 May 2024).
23. Feng, K.; Li, M.; Liu, W.; Kashkooli, A.G.; Xiao, X.; Cai, M.; Chen, Z. Silicon-Based Anodes for Lithium-Ion Batteries: From Fundamentals to Practical Applications. *Small* **2018**, *14*, 1702737. [CrossRef] [PubMed]
24. Tang, J. Progress in the application of silicon-based anode nanotechnology in lithium batteries. *E3S Web Conf.* **2024**, *553*, 01007. [CrossRef]
25. Avanzini, G.; de Angelis, E.L.; Giulietti, F. Optimal performance and sizing of a battery-powered aircraft. *Aerosp. Sci. Technol.* **2016**, *59*, 132–144. [CrossRef]
26. Zhou, Y.; Zhao, H.; Liu, Y. An evaluative review of the VTOL technologies for unmanned and manned aerial vehicles. *Comput. Commun.* **2020**, *149*, 356–369. [CrossRef]
27. Full Report—Study on the Societal Acceptance of Urban Air Mobility in Europe. Available online: https://www.easa.europa.eu/en/full-report-study-societal-acceptance-urban-air-mobility-europe (accessed on 13 June 2024).
28. Çetin, E.; Cano, A.; Deransy, R.; Tres, S.; Barrado, C. Implementing Mitigations for Improving Societal Acceptance of Urban Air Mobility. *Drones* **2022**, *6*, 28. [CrossRef]
29. Mazzeo, F.; Pavel, M.D.; Fattizzo, D.; Bertolani, G.; de Angelis, E.L.; Giulietti, F. Flight dynamic modeling and stability of a small-scale side-by-side helicopter for Urban Air Mobility. *Aerosp. Sci. Technol.* **2024**, *148*, 109117. [CrossRef]
30. Fast-Forwarding to a Future of On-Demand Urban Air Transportation. Available online: https://uberpubpolicy.medium.com/fast-forwarding-to-a-future-of-on-demand-urban-air-transportation-f6ad36950ffa (accessed on 8 August 2024).
31. Sagaga, J.; Lee, S. Acoustic predictions for the side-by-side air taxi rotor in hover. In Proceedings of the AIAA Aviation Forum, San Diego, CA, USA, 12–16 June 2023
32. Abalakin, I.A.; Bobkov, V.G.; Kozubskaya, T.K. Numerical Study of Fuselage Impact on Acoustic Characteristics of a Helicopter Rotor. *J. Supercomput.* **2022**, *9*, 100–113.
33. Yin, J. Investigation of rotor noise shielding effects by the helicopter fuselage in forward flight. *J. Aircr.* **2019**, *56*, 1677–1688. [CrossRef]
34. Brentner, K.S.; Farassat, F. Helicopter Noise Prediction: The Current Status and Future Direction. *J. Sound Vib.* **1994**, *170*, 79–96. [CrossRef]
35. Yunus, F.; Casalino, D.; Avallone, F.; Ragni, D. Efficient prediction of urban air mobility noise in a vertiport environment. *Aerosp. Sci. Technol.* **2023**, *139*, 108410. [CrossRef]
36. Kopiev, V.F.; Zaytsev, M.Y.; Vorontsov, V.I.; Karabasov, S.A. Helicopter noise in hover: Computational modelling and experimental validation. *Acoust. Phys.* **2017**, *63*, 686–698. [CrossRef]
37. Smith, B.; Gandhi, F.; Niemiec, R. A comparison of multicopter noise characteristics with increasing number of rotors. In Proceedings of the 76th Annual Forum of the Vertical Flight Society, Virtual, 5–8 October 2020.
38. Kadhiresan, A.R.; Duffy, M.J. Conceptual design and mission analysis for eVTOL Urban Air Mobility flight vehicle configurations. In Proceedings of the AIAA Aviation Forum, Dallas, TX, USA, 17–21 June 2019.